BJRS

BRAZILIAN JOURNAL
OF
RADIATION SCIENCES
10-03 (2022) 01-17

Dosimetric assessment and secondary cancer risk in breast radiotherapy: a Monte Carlo approach

Faés[a] G.R.S.0, Santos[b] W.S., Alva-Sánchez[a] M.S., Alva[a] T.A.P.

[a] *Universidade Federal de Ciências da Saúde de Porto Alegre (UFCSPA)/ Departamento de Ciências Exatas e Sociais Aplicados, 90050-170, Porto Alegre, Rio Grande do Sul, Brasil*

[b] *Universidade Federal de Uberlândia (UFU)/ Instituto de Física, 38.400-902, Uberlândia, Minas Gerais, Brasil*

giulia.faes@edu.pucrs.br

ABSTRACT

This work aimed to calculate the risk of secondary cancer induction due to a breast radiotherapy scenario simulating. MCNPX 2.7.0 code and voxel-based anthropomorphic phantom were used to simulate static MLC in the 3D-CRT technique for a case of breast radiotherapy. The simulation results can determine the radiation dose in organs and tissues. The adult anthropomorphic phantom FSTA_H50_M50 was used. A LINAC Varian 2100C device that can operate with two techniques was simulated: 2D with open field (OF) and 3D-conformational (3D-CRT), the latter with the use of a multileaf collimator (MLC), both for 6 MV therapeutic beam. The highest values of absorbed dose were obtained for the ipsilateral lung of 7.22 Gy (3D-CRT) and 8.49 Gy (OF) and for the contralateral breast of 6.29 Gy (3D-CRT) and 6.56 Gy (OF), which can be inducing highest risks of secondary cancer. Since the OF technique, non-collimation of the beam, there was an increase in the absorbed dose for all organs compared to the 3D-CRT procedure. Thus, it is evident that treatments with the 3D-CRT technique are safer, improving both homogeneity and conformity with the absorbed dose to the target organ.

Keywords: **breast cancer, dosimetry, anthropomorphic phantom, Monte Carlo simulation.**

ISSN: 2319-0612
DOI: https://doi.org/10.15392/bjrs.v10i3.2064
Submitted: 2022-05-16
Accepted: 2022-09-05

1. INTRODUCTION

Cancer is a pathology of multiple causes, such as environmental, cultural, and socioeconomic factors, lifestyles, and even hereditary factors. Neoplasms proliferated worldwide, occupying the second leading cause of death in almost all countries. In the short term, it is projected that cancer will surpass cardiovascular diseases in developed countries [1]. The publication by the National Cancer Institute (INCA), a federal institution in Brazil, showed that from 2020 to the present, there was an estimated incidence of 309,750 new cancer cases in men and 316,280 in women in Brazil [2]. Furthermore, it establishes that in the world, lung cancer is the most common (2.1 million cases), followed by breast cancer (2.1 million cases), colon and rectum (1.8 million cases), and finally, prostate (1.3 million cases) [2]. In Brazil (the estimate for the period 2020-2022), the most common cancer is non-melanoma skin (177 thousand new cases), followed by prostate and breast cancers (66 thousand new cases each). In 2018, the world estimate showed 9.6 million deaths [2].

The growing number of breast cancer cases is a similar outlook across the world. Breast cancer is the most prevalent cancer affecting women worldwide in developed and developing countries. This neoplasm is also considered the leading cause of death among women of a specific age group, especially during menopause [2]. It is worth mentioning that, according to the INCA [3], the estimate for 2020 was 66,280 new breast cancer cases and the estimated number of deaths per year is 16,927 (16,724 women and 203 men).

After breast cancer diagnosis, numerous methods are discussed among the various forms of treatment: radiotherapy, chemotherapy, hormone therapy, biological therapy, and surgery. Among these, radiotherapy is one of the most used. Even recognizing its benefits, radiotherapy inevitably exposes organs and tissues that are totally or partially not included in the treatment planning. In this sense, it is essential to know with a certain precision the dose that will be delivered to the target organ and other organs and tissues located outside the patient's treated region. As seen in Santos *et al.* [4] study, conventional two-dimensional plans (2D) are based on standard radiographs and the conformation of the dose is achieved through collimation blocks. The 3D-CRT technique is performed using multileaf collimators (MLC), forming the bundle in the target region, thus saving

adjacent healthy tissues; also, in the 3D-CRT approach, the dose distribution calculation is obtained through tomographic acquisitions, thus acquiring optimized clinical results [4].

However, information on doses in healthy organs located near or far from the treated region is poorly reported in the literature. The studies show considerably higher doses for organs and structures close to the irradiation field.

Gonzalez *et al.* [5] report a high risk of inducing secondary cancer for doses greater than 1 Gy received by the ipsilateral lung and esophagus during breast cancer treatment. Stovall *et al.* [6] showed that women under 40 are more likely to develop contralateral breast cancer when the dose in the healthy breast is greater than 1 Gy. Huang and Mackillop [7] reported an elevated risk of soft tissue sarcomas located in the vicinity of the treatment volume. In addition to the radiosensitive organs closest to the region treated as the thyroid, esophagus, lungs, and heart. In addition to these organs, other more distant organs, such as salivary glands and ovaries, are likely to develop secondary cancer resulting from scattered radiation from the irradiated [7,8].

One of the difficulties in assessing the risk of secondary cancer is the lack of dose values in the organs. However, a viable alternative to solve this problem is using anthropomorphic simulators in conjunction with a radiation transport code.

The Monte Carlo N-Particle extended (MCNPX) code [9] is a tool used in several areas of science, especially in Medical Physics, which models radiation scenarios for radiotherapy treatments, taking into account the anatomical and morphological heterogeneity of the desired structures [10]. According to Mendes *et al.* [11] methodology, assessed the absorbed dose in the body's organs during the simulation of a three-dimensional (3D) radiotherapy of the breast, using the MCNP code, reported a higher risk of secondary cancer incidence for the contralateral breast, followed by blood-forming tissues, lungs, and stomach. In addition, other researchers appraised the dose absorbed in other organs as a result of breast cancer radiotherapy [12, 13]. Therefore, the original contribution of this work is the use of anthropomorphic phantoms based on voxel and the use of Linac MLCs. Taghavi *et al.* [12] used ORNL mathematical phantoms and Toosi *et al.* [13] used the Randon phantom.

The importance of the study in realizing this methodology is verified, given the scarcity of studies related to the risk of secondary cancer induced due to breast cancer radiotherapy, being a strong motivation for the present study.

The current work aims to calculate the risk of secondary cancer induction through a Monte Carlo simulation code and voxel-based anthropomorphic phantom to determine the radiation dose in organs and tissues.

2. MATERIALS AND METHODS

In this work MCNPX code (version 2.7.0) [9] was used to model the exposure scenarios of a breast radiotherapy procedure treated with a medical linear accelerator (LINAC) developed by Bernarz *et al*. [14] and adapted for this study. Two treatment models were considered: 3D-CRT (conformed to MLC) and 2D with open field (OF). The patient was represented by an anthropomorphic computer phantom, called FSTA_H50_M50, which was built by the Computational Dosimetry Group of the Department of Nuclear Energy at the Federal University of Pernambuco, Brazil [15]. This phantom object is 1.63 m tall and has a 65 kg body weight. It includes more than one hundred structures with dosimetric importance, including all the risk organs recommended by the International Commission of Radiological Protection 103 (ICRP) [16]. This phantom object's organs, tissues, and other structures are formed by voxels of dimensions (2.4 x 2.4 x 2.4) mm. The primary information used in the context of radiation transport is shown in Table 1.

Table 1: Details of the methodologies used in Monte Carlo simulation processes.

Item	Description	References
Code and version	MCNPX version 2.7.0	[9]
Source description	LINAC is operated with a 6 MV photon beam, jaws, and an 80-sheet MLC. The primary and secondary collimators and the other structures affecting scattered radiation were considered. The energy spectrum used was obtained from the reference [17].	[4, 14]
Cross Sections	ENDF/B-VII	[9]
Transport parameters	The photon and electron transport were performed with cutting energy of 0.01 MeV for photons and 0.1 MeV for electrons. Photon transport was considered to include both photoelectric absorption with the possibility of fluorescent and Auger electron emission and Compton scattering	[9]
Dose recording	Tally F6, the dose absorbed in a cell (in MeV/g/particle), was used to obtain doses in the organs and tissues of interest. For the calculation of the percentage of depth dose (PDD) and dose profiles, tally *F8 (MeV/particle) was used. Tally F4, in MeV/cm³/particle, was used to generate the photon energy fluence and evaluate the beam's collimation.	[9]
Number of particle histories and relative errors	In all scenarios, 1E+08 particle histories were used. In all output files, the relative errors were less than 5% for both the organs located within the target region and those distant.	[9]
Data post-processing	The absorbed dose for each organ and tissue was normalized relative to the target organ, the left breast. This ratio, called the conversion factor (CF), was multiplied by the prescribed treatment dose, thus obtaining the absorbed dose in each organ and tissue.	

2.1. Description of the computational model

Figure 1 presents the computational scenario with LINAC operating with MLC (Figure 1 (a)) and OF (Figure 1 (b)), respectively, with the patient in the supine position on a positioning table. The LINAC head is also presented. The table is 10 cm thick, 70 cm wide and 200 cm long and made of carbon fiber. A metallic base maintains it. In addition to the secondary collimators used to form an open rectangular field of dimensions (10 x 16) cm² in the internal tangential projections with a gantry angle of 110º and external tangential with 308º, a collimation system used in modern

accelerators operating in 3D-CRT was also developed with dimensions comparable to the size of the breast. In this study, the MLC consists of two sets of 80 sheets of lead distributed diametrically opposite [4, 14].

Figure 1*: Computational model, simulated in the MCNPX, of exposure in a breast radiotherapy procedure.*

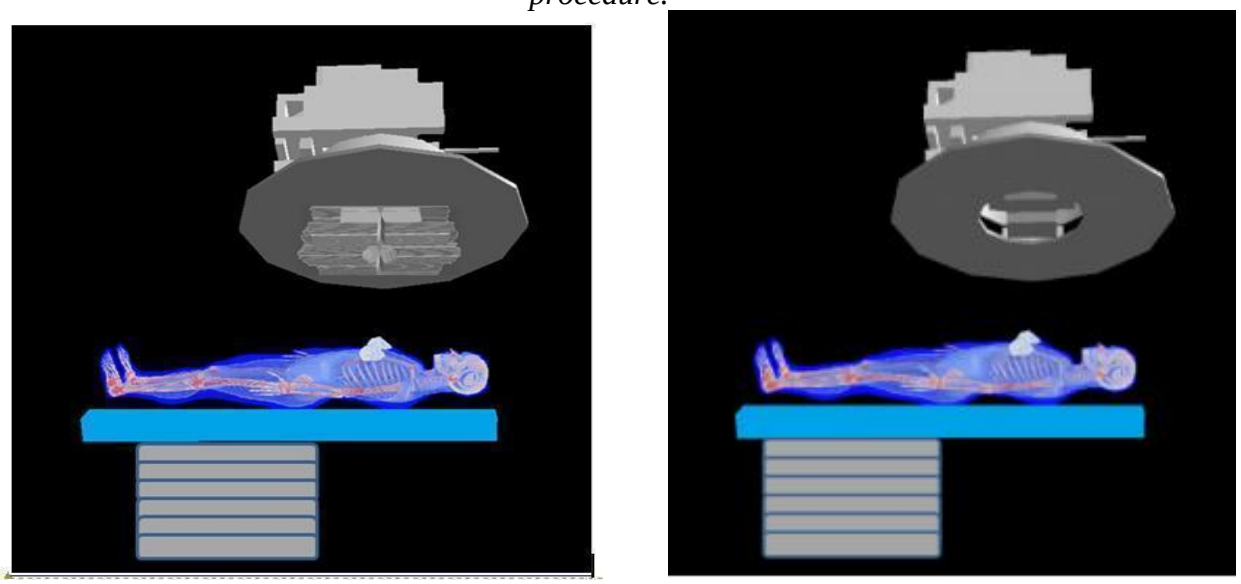

(a) Conformational 3D (b) Open field

Two opposing tangential fields (external and internal) were used during the treatment simulation. The same field size (10 x 16) cm^2 was used for both fields. However, we did two simulations, one with the usual OF treatment (two opposing tangential fields with field opening (10 x 16) cm^2) and the other using the MLC technique in a 3D-CRT treatment. The radiation field was directed to the left breast [18].

Tally F4 (in MeV/cm^3/particle) from the MCNPX code was used to generate the photon energy fluence and evaluate the beam's collimation.

2.2. Evaluation of beam properties

The MCNPX Monte Carlo code was used to simulate the transport of radiation through the complex geometry of the LINAC head and the patient's anatomy.

The beam properties were validated through the PDD and the dose profile comparisons with clinical data obtained at the radiotherapy service of the Santa Casa of Misericórdia of Porto Alegre (Brazil). The simulation results were obtained with the tally *F8 (MeV/source/particle) for the evaluation of the energy deposited in the water along the central axis of the beam. To determine the PDD and the dose profile values, it was necessary to model a set of voxels to represent the radiation detectors distributed along the central axis and the axial axis. The first set consists of exactly 400 voxels distributed along the central axis and the second with 100 voxels along the axial axis. The energy deposited in each voxel of the central axis and the axial axis at the maximum dose depth was used to determine the PDD and the dose profile, respectively.

PDD calculations were made with 1 mm spacing between detectors. Both simulations were performed using a polymethylmethacrylate (PMMA) phantom of dimensions (30 x 30 x 30) cm^3 filled with water with walls 1 cm thick and with voxel dimensions of (2.5 x 2.5 x 0.1) cm^3 for assessment of PDD and (1 x 1 x 0.4) cm^3 for evaluation of the dose profile. The LINAC Varian 2100C was operated with a nominal energy of 6 MV with the photon beam generating a field of (10 x 10) cm^2 at a source-surface distance (SSD) of 100 cm. Figure 2 shows the computational model used to determine these two parameters.

Figure 2: *Computational model, simulated in the MCNPX, used to determine both the PDD (yellow line) and the dose profile (red line) of the beam.*

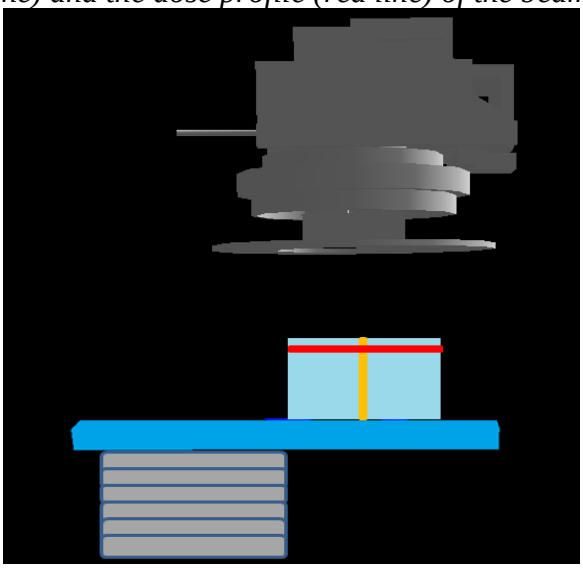

PDD and dose profile measurements were performed using the Farmer ionization chamber (PTW model) with a sensitive volume of 0.6 cm^3. PDD was measured with the camera positioned along the central axis with depths ranging from 0 to 20 cm with steps of 0.5 cm; the dose profile was measured along the axial axis from -10 to 10 cm with 0.4 cm steps. Both parameters were normalized by the absorbed dose at a depth of 1.5 cm in the central axis [4, 14, 18].

2.3. Dosimetric calculations

In this study, a set of absorbed doses in organs and tissues located in or near the target volume during radiotherapy for left-sided breast cancer was determined for a 35-year-old adult patient. The dosimetric results were due to the primary photons and scattered secondary electrons. Regarding the absorbed doses by organs and tissues with dosimetric importance recommended by the ICRP [16], it was calculated using Equation 1. The treatment prescribed by Rudra *et al.* [19] delivered 50.4 Gy to the left breast tumor region. This amount was divided into 28 fractions, 1.8 Gy per day.

$$D(Gy) = \frac{D_T}{D_C}\ x\ D_P \qquad (1)$$

D_T is the estimated absorbed dose in each organ and tissue T, D_C the dose in left breast volume, and D_P the total dose prescribed for the treatment of radiotherapy. This study's, the $\frac{D_T}{D_C}$ ratio is called the conversion factor (CF).

3. RESULTS AND DISCUSSION

3.1. Dosimetric properties of the simulated radiation beam

Figure 3 shows the comparison between the PDD curve obtained through the MCNPX code and the measurement with the ionization chamber with the respective difference between them. Both were obtained with reference parameters, for various depths in the water phantom object. The results were normalized to the corresponding dose at the maximum dose depth. The average percentage difference between the experimental and simulated results was 2.5% for the post-build-up region and less than 3.6% for the pre-build-up region.

Figure 3: *PDD curves simulated (red) using the MCNPX code and (blue) experimental, obtained with 6 MV photon beam and irradiation field (10 x 10) cm².*

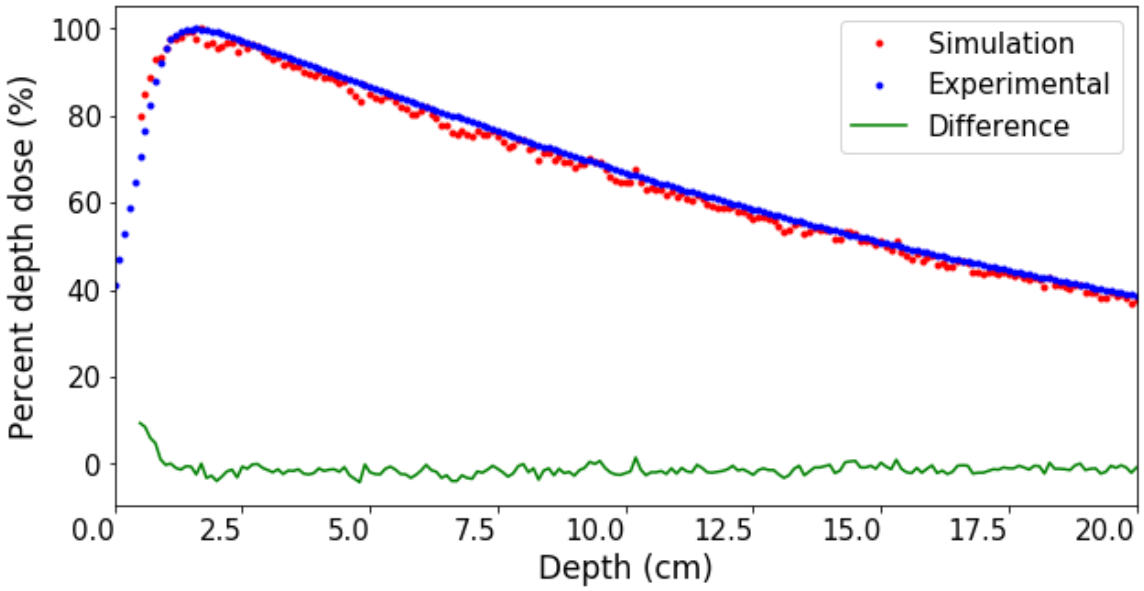

The dose profiles, simulated and experimental, were obtained at the maximum dose depth and are shown in Figure 4, together with the difference between them. The average difference between the experimental and simulated values was less than 1.1% for the irradiation field region, that is, -4.4 to 4.4 cm. This sharp 6% error between -5.3 to -4.5 cm and between 4.5 to 5.3 cm may be associated with the position of the detectors. For the high dose gradient region, it is impossible to correctly estimate the differences since a slight variation in position results in a significant difference in the amount of the deposited dose in this region.

Figure 4: *Dose profile curve (red) simulated using the MCNPX code and (blue) experimental, obtained with 6 MV photon beam and irradiation field (10 x 10) cm².*

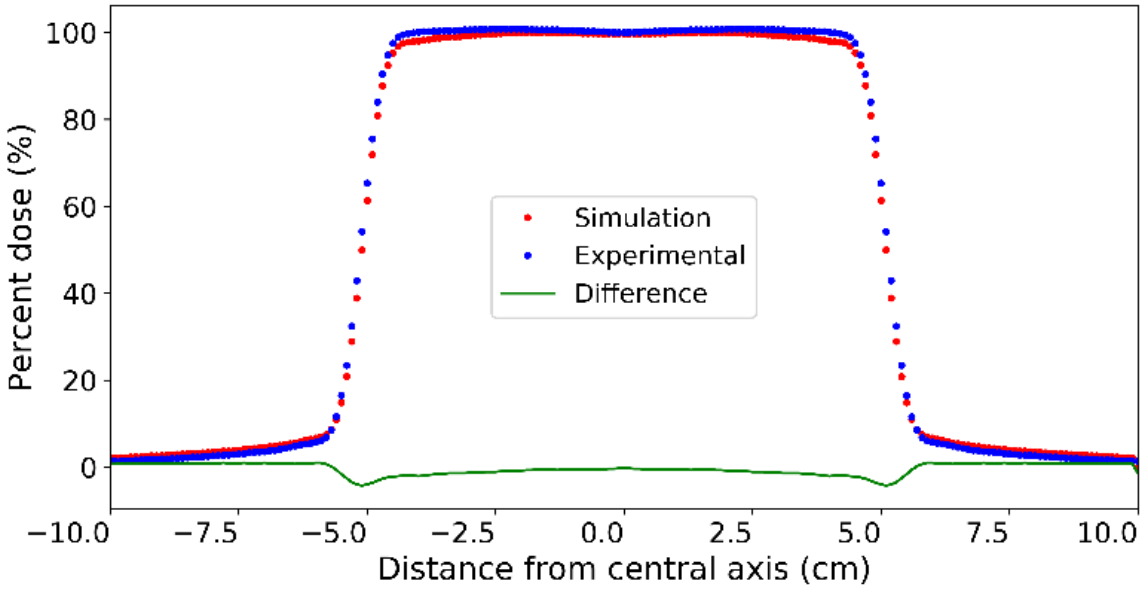

3.2. Dosimetric evaluation using the anthropomorphic phantom FSTA_H50_M50

Table 2 presents the results of the conversion factors (CFs) of the absorbed dose of a set of organs and tissues with dosimetric importance. These CFs were calculated by normalizing the absorbed doses of non-target organs and tissues by the absorbed dose of the left breast, the target organ affected by cancer [20]. Through the CFs, it was possible to obtain the average absorbed dose for each organ and tissue of the two beam projections studied. The results of the average absorbed dose for the treatments with the field modulated by the 3D-CRT technique and OF (10 x 16) cm² with their respective dose relative error (between parentheses) are shown in Table 2.

Table 2: Conversion factor (CF) (in units of Gy/Gy) and average absorbed dose (in unit Gy) for the 3D-CRT and OF techniques. In parentheses are the relative errors.

	Conversion factor (CF)					
	10x16 3D-CRT			**10x16 OF**		
Organs	**Internal tangencial**	**Extgernal tangencial**	**Average absorbed dose**	**Internal tangencial**	**Extgernal tangencial**	**Average absorbed dose**
Red bone marrow	7.60E-03 (0.09%)	1.66E-02 (0.06%)	6.11E-01	1.00E-02 (0.08%)	1.92E-02 (0.06%)	7.36E-01
Colon	1.47E-03 (0.49%)	1.45E-03 (0.50%)	7.35E-02	2.49E-03 (0.42%)	2.60E-03 (0.40%)	1.29E-01
Right lung	7.67E-03 (0.19%)	3.72E-03 (0.28%)	2.87E-01	9.88E-03 (0.18%)	4.76E-03 (0.26%)	3.69E-01
Left lung	8.03E-02 (0.09%)	2.06E-01 (0.07%)	7.22E+00	9.69E-02 (0.09%)	2.41E-01 (0.07%)	8.49E+00
Stomach	6.61E-03 (0.38%)	3.77E-03 (0.46%)	2.62E-01	9.02E-03 (0.34%)	5.18E-03 (0.43%)	3.58E-01
Gonads	4.27E-04 (4.63%)	5.40E-04 (3.85%)	2.44E-02	1.02E-03 (3.04%)	1.36E-03 (2.52%)	6.00E-02
Bladder	3.26E-04 (2.87%)	4.31E-04 (2.87%)	1.91E-02	8.37E-04 (1.84%)	1.13E-03 (1.91%)	4.97E-02
Esophagus	8.11E-03 (0.52%)	6.82E-03 (0.50%)	3.77E-01	1.10E-02 (0.48%)	8.81E-03 (0.47%)	4.99E-01
Liver	2.03E-02 (0.17%)	4.26E-02 (0.13%)	1.59E+00	5.19E-02 (0.14%)	8.79E-02 (0.10%)	3.52E+00
Thyroid	2.38E-03 (1.50%)	2.95E-03 (1.36%)	1.34E-01	3.59E-03 (1.32%)	4.39E-03 (1.19%)	2.01E-01
Brain	5.00E-04 (0.96%)	5.31E-04 (0.79%)	2.60E-02	1.32E-03 (0.63%)	1.22E-03 (0.61%)	6.42E-02
Skin	3.73E-02 (0.06%)	3.73E-02 (0.06%)	1.88E+00	4.32E-02 (0.06%)	4.18E-02 (0.06%)	2.15E+00
Heart	1.75E-02 (0.25%)	8.57E-03 (0.29%)	6.56E-01	2.24E-02 (0.23%)	1.12E-02 (0.28%)	8.47E-01
Salivary glands	1.58E-03 (0.98%)	1.42E-03 (1.02%)	7.56E-02	3.08E-03 (0.76%)	2.77E-03 (0.87%)	1.48E-01
Adrenal glands	6.55E-03 (1.00%)	6.93E-03 (0.91%)	3.40E-01	8.86E-03 (0.94%)	9.37E-03 (0.82%)	4.59E-01
Extrathoracic region	1.41E-03 (1.76%)	1.46E-03 (1.51%)	7.24E-02	2.82E-03 (1.35%)	2.70E-03 (1.22%)	1.39E-01
Gallbladder	5.67E-03 (0.87%)	4.99E-03 (0.91%)	2.69E-01	8.13E-03 (0.78%)	7.13E-03 (0.81%)	3.85E-01
Right kidney	3.21E-03 (0.71%)	2.44E-03 (0.74%)	1.43E-01	4.33E-03 (0.63%)	3.35E-03 (0.66%)	1.94E-01
Left kidney	4.29E-03	6.80E-03	2.80E-01	6.41E-03	9.30E-03	3.96E-01

	(0.65%)	(0.45%)		(0.55%)	(0.40%)	
Eyes	8.21E-04	7.77E-04		1.87E-03	1.95E-03	
	(2.87%)	(3.01%)	4.03E-02	(2.13%)	(2.10%)	9.64E-02
Uterus	4.13E-04	5.24E-04		1.02E-03	1.24E-03	
	(2.20%)	(1.93%)	2.36E-02	(1.61%)	(1.58%)	5.69E-02
Soft tissue	2.81E-02	3.60E-02		3.41E-02	4.01E-02	
	(0.07%)	(0.06%)	1.61E+00	(0.06%)	(0.06%)	1.87E+00
Bone surface	8.27E-03	1.80E-02		1.09E-02	2.08E-02	
	(0.09%)	(0.06%)	6.63E-01	(0.08%)	(0.06%)	8.00E-01
Right breast	2.45E-01	5.54E-03		2.52E-01	8.13E-03	
	(0.12%)	(0.49%)	6.29E+00	(0.12%)	(0.44%)	6.56E+00
Left breast	1.00	1.00		1.00	1.00	
	(0.07%)	(0.07%)	5.04E+01	(0.07%)	(0.07%)	5.04E+01
Trachea	5.52E-03	5.25E-03		7.48E-03	6.73E-03	
	(0.94%)	(0.82%)	2.72E-01	(0.83%)	(0.75%)	3.58E-01
Lymph nodes	9.28E-03	4.72E-02		1.28E-02	5.22E-02	
	(0.18%)	(0.11%)	1.42E+00	(0.15%)	(0.10%)	1.64E+00
Muscle	2.58E-02	3.58E-02		3.18E-02	4.04E-02	
	(0.07%)	(0.06%)	1.55E+00	(0.06%)	(0.06%)	1.82E+00
Buccal cavity	1.61E-03	1.32E-03		3.10E-03	2.79E-03	
	(1.31%)	(1.44%)	7.40E-02	(1.10%)	(1.30%)	1.49E-01
Pancreas	3.52E-03	2.96E-03		5.02E-03	4.30E-03	
	(0.72%)	(0.67%)	1.64E-01	(0.63%)	(0.59%)	2.35E-01
Small	1.01E-03	1.14E-03		1.96E-03	2.28E-03	
intestine	(0.61%)	(0.55%)	5.42E-02	(0.52%)	(0.43%)	1.07E-01
Spleen	5.26E-03	2.75E-03		7.03E-03	3.58E-03	
	(0.58%)	(0.93%)	2.02E-01	(0.53%)	(0.84%)	2.67E-01
Thymus	2.95E-02	1.05E-02		4.10E-02	1.39E-02	
	(0.54%)	(0.64%)	1.01E+00	(0.49%)	(0.61%)	1.39E+00
Bronchi	9.32E-03	9.51E-03		1.26E-02	1.18E-02	
	(0.73%)	(0.51%)	4.75E-01	(0.66%)	(0.47%)	6.16E-01
Blood	1.18E-02	1.99E-02		1.65E-02	2.29E-02	
	(0.22%)	(0.11%)	8.03E-01	(0.19%)	(0.11%)	9.92E-01

Table 2 shows that the left lung, liver, and right breast are the organs that receive the highest doses. For 3D-CRT treatment, a dose of 7.22 Gy was verified for the left lung, 6.29 Gy for the right breast, and 1.59 Gy for the liver. For OF technique, 8.49 Gy for the left lung, 6.56 Gy for the right breast, and 3.52 Gy for the liver. It is common in breast cancer treatments that a portion of the lung is exposed due to its anatomical location. The doses for the liver and the opposite breast are due to

the anatomical positions, consequent the gantry positioning for the irradiation of the target breast, allowing dose radiation to reach a portion of these organs.

These three organs received the highest total absorbed doses. About the left lung, the dose absorbed by the organ can cause irreversible damage, both functional and radiological, without any association with clinical symptoms. Some of the recurrent changes in patients are increased density, symptomatic radioactive pneumonitis (fever, cough, and dyspnea), increased pulmonary clearance, and quantitative reduction in lung function tests. Thus, it became evident that breast cancer radiotherapy can cause a decrease in inspiratory and vital capacity, interfering with lung volume and respiratory muscle strength [21]. As for the liver, as Hormati et al. [22] reported, there is no significant relationship between breast cancer radiotherapy and the development of liver fibrosis. Despite the recommended care in case of any liver function disorder, there is no report of effect on liver stiffness.

The relative dose error for each field (external and internal tangential) was calculated considering the biggest one for the 3D-CRT treatment (4.6%) and OF (3.0%)—both for the internal tangential field in the region of the gonads. The therapy with OF has a lesser relative error in the simulation associated with the deposited dose and the number of particles simulated because when the dose in a region is higher, the relative error will be minor.

In radiotherapy centers, after planning, the dose values that each volume of a given organ can receive are checked based on dose constraints. This analysis was performed using the dose-volume histogram (DVH). In Table 2, accomplished both plans were for the ipsilateral lung since 100% of the volume of the left lung received 7.22 Gy (3D-CRT) and 8.49 Gy (OF); for the opposite breast, 100% of its volume received 6.29 Gy (3D-CRT) and 6.56 Gy (OF), therefore, it surpassed the restrictions, since we consider the whole organ. The dose constraints were similar to the contralateral breast's limit V5Gy $\leq$ 15% and the ipsilateral lung's limitation V20Gy $\leq$ 45% for a total treatment dose of 50.4 Gy [19].

In the 3D-CRT for breast treatment, the patient’s chest contour is defined, including both the target and the risk organs, such as the ipsilateral lung, contralateral breast, and heart. In this technique, two opposing parallel tangent fields are used to guarantee the best breast coverage, thus minimizing the dose to the organs at risk. With the change of the OF to 3D-CRT, there was a reduction in the absorbed dose in all organs.

This reduction was over 3% for the right breast, over 14% for the left lung, and over 50% for the gonads, bladder, liver, brain, eyes, and uterus. That's because the advent of 3D-CRT allowed visualization of the tumor and the normal structures and can be identified with better precision. Also, the technique has the advantage of being able to assess and enable the reduction or prevention of the potential toxicity of radiotherapy [23].

In particular, the concave shape of the chest wall and the contralateral breast causes irradiation in areas of the ipsilateral lung and heart. These organs are situated to the left of the trunk. 3D-CRT radiotherapy, on the other hand, attenuates these effects by increasing the degrees of freedom in the planning process, thus enabling greater dose homogeneity, reducing the irradiation of healthy tissues and high-dose regions, responsible for the increase in the acute and late effects of radiation, such as fibrosis, telangiectasia, wet peeling among others. These effects can be even more significant in women with large breasts.

Regarding the difference in the average absorbed dose between the treatment with the 3D-CRT technique and with OF, it was possible to verify that the bladder and uterus present the most considerable dose difference, 62% and 59%, respectively [19]. This evidences that the treatment with 3D-CRT is preferable because it reduces the dose delivered to these organs. Since this difference, there was a decrease in the dose compared to the 3D-CRT and OF planning. Furthermore, they are small organs, naturally shielded by other structures and located far from the target volume. There is little scattered radiation; the relative uncertainty is high, generating a more significant dose difference. These results are in agreement when comparing dose distribution of the 3D-CRT between the 2D technique from the chest wall of patients with post-mastectomy breast cancer; showing that the 3D-CRT process has a significantly better homogeneity index than PTV, with a reduction in the average doses of the ipsilateral lung and the heart. It is essential to verify that with or without MLC, the dose in the target remains the same since it was normalized to get the maximum dose.

With the use of OF, the field of view is more extensive; consequently, there is a greater irradiated area, darkness, and scattered radiation in areas more distant from the target. Furthermore, the dose gradient is high in planning the OF technique, and the isodoses are more comprehensive since there is no dose conformation, unlike treatment with 3D-CRT. However, the MLCs used in the 3D-CRT technique are rounded. This format prevents discontinuity between the radiation field

and the light projection; compared to blades with diverging edges, those with rounded edges increase the percentage of photon transmission. Thus, causing a more blurred field boundary and being responsible for producing a more significant amount of indirect photons and electronic contamination

3.3. Secondary cancer risk

Regarding the risk of cancer (R_E), it is calculated using Equation 2 [24],

$$R_E = \sum r_T \; x \, H_T \tag{2}$$

where H_T is the equivalent dose in the organ and tissue of interest and r_T is the cancer risk coefficient [25] for a 35-year-old woman with cancer in the left breast. The r_T is the cancer risk coefficient attributable throughout life for the number of cases of cancer incidence per 100,000 people exposed to a single dose of 0.1 Gy.

The BEIR VII methodology (Health Risks from Exposure to Low Levels of Ionizing Radiation) was used to analyze the selected organs. BEIR VII is a committee of the National Academy of Sciences in charge of studying and estimating the detailed risks for cancer incidence. In addition to cancer mortality and other health effects of exposure to low-level and ionizing radiation [25]; however, the approach is generally valid only for absorbed doses below 1.0 Gy. Thus, only the average absorbed dose of the organs in question was considered when estimating the risk [11].

Figure 5 shows the risks of cancer incidence for a set of organs and tissues depending on the type of treatment. It is possible to compare the association with a group of selected organs for 3D-CRT plannings and the OF.

Figure 5: *Risk of secondary cancer induction related to a group of selected organs.*

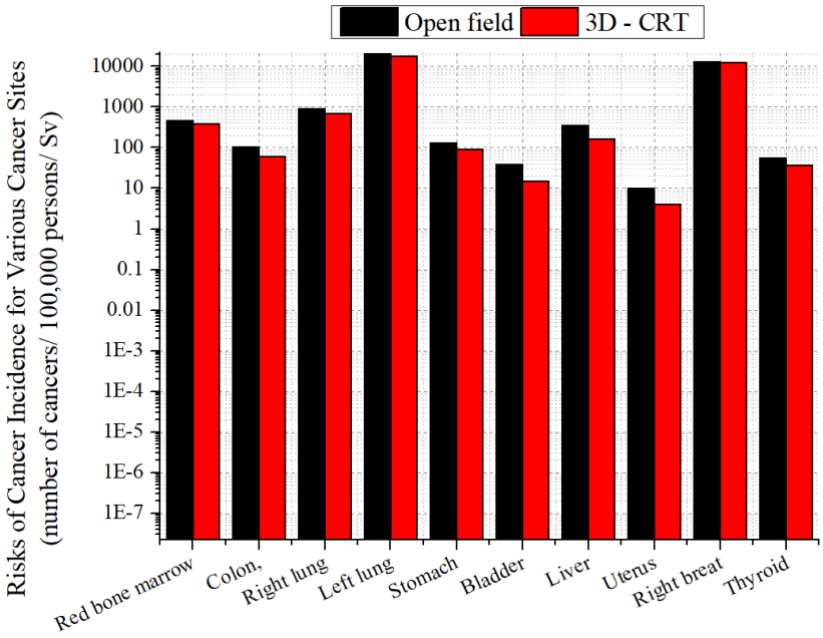

In both plans, the organs with the largest R_E were the ipsilateral lung and the contralateral breast, as also reported by Mendes *et al.*[11], which found, for the 3D-CRT technique, a larger R_E for the contralateral breast and lung. This is due to the proximity of both organs to the target, causing them to receive a larger dose. It is also possible to verify that no linearity between the organs obtained the highest values of average absorbed dose and the highest values of cancer risk since there is dependence on r_T, which varies depending on the analyzed organ.

In Mendes et al. [11] work, there are only 63 different organs and tissues, and the simulator is represented by a woman 165 cm tall and 98 kg. The size of the voxel he used was (5 x 5 x 5) mm^3, with the left breast being chosen for irradiation, presenting a high risk of cardiac involvement. Two opposing parallel tangent beams and 100 cm SSD were used. Mendes et al.[11] made use of 15º filters, a fact that may have influenced the irradiation of some organs, thus obtaining values different from those obtained in the present study.

Regarding the radiation received by the contralateral breast, Hormati et al. [22] analyze breast cancer radiotherapy's contribution to the risk of second cancer in the opposite breast. As a result, less than 3% was attributed to radiotherapy treatment for developing second cancer.

Regarding the difference in cancer risk induction between 3D-CRT and OF, the smallest differences are found for organs closer to the left breast, observing 4% for the right breast and 15%

for the left lung. Because scattered radiation contributes to more distant organs, which can modify depending on the collimation (Figure 6), the closest organs are directly affected, mainly by radiation. Consequently, without much difference in dose associated with them, as observed in the difference in dose absorbed for the left lung and the contralateral breast. It is also possible to verify, in a panoramic view of the patient's anatomy (Figure 6), that both the left lung and the right breast are close to the irradiation field, often within the planned target volume (PTV), receiving thus, radiation in a primary form. Unlike distant organs that secondarily receive the dose due to the amount of radiation spread within the body of the simulator object.

Figure 6: *Collimation of the beam for OF and 3D-CRT in the internal tangential (left) and external tangential (right) views, respectively.*

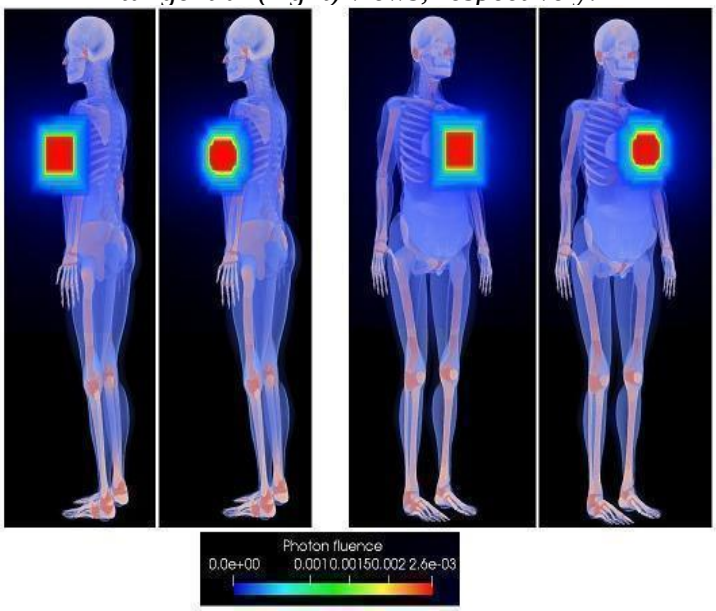

4. CONCLUSION

In this study, using MC simulation, conversion factors were determined for the absorbed dose in a set of organs and/or tissues of the anthropomorphic phantom, representing an adult woman undergoing treatment for left breast cancer. The modeled computational scenario was composed of the phantom and the head of the medical linear accelerator (LINAC) Varian 2100C with a 6 MV

photon beam. The precise knowledge of the conversion factors made it possible to calculate the absorbed doses for a set of organs and tissues. As expected and proven, most organs close to or within the target volume received the highest doses of radiation, including the left lung and right breast. The choice of the technique used for the treatment considerably affects the results. It noticed a reduction of the R_E, for the selected organs by approximately 38% between one technique and another, being the OF technique had the biggest R_E. Usually, the absorbed dose by the organs depends highly on their distance from the target, their locations, and distributions in the body. Comparing the R_E (number of cancer cases / 100,000 persons/Sv) values for each technique used, it was observed that both, the left lung (1.74E + 04 and 2.05E + 04) and the contralateral breast (1.24E + 04 and 1.29E + 04) had the highest R_E for the 3D-CRT and OF technique, respectively, since these were also the organs that received the highest absorbed doses. The 3D-CRT technique allows the use of computer systems for planning, thus performing the 3D-CRT in the PTV, considerably improving the dose deliveries, making it more homogeneous; the organs close to the target and the healthy tissues that, with a OF treatment, received high doses, received lower doses with 3D-CRT.

ACKNOWLEDGMENT

The authors would like to thank the Radiotherapy Service of Irmandade da Santa Casa de Misericórdia de Porto Alegre (ISCMPA) for kindly providing the clinical data used in this work. To CNPq for the computational resources made available through the project 427273 / 2016-1 of the Universal Call, and CNPq, research productivity grant project nº 309675/2021-9.

REFERENCES

[1] OLIVEIRA, M. M. D.; MALTA, D. C.; GUAUCHE, H.; MOURA, L.; SILVA, G. A. Estimated number of people diagnosed with cancer in Brazil: data from the national health survey, 2013. **Rev Bras Epidemiol.,** v. 18, p. 146-157, 2015.

[2] INCA – Instituto Nacioanal do Câncer (National Cancer Institute)**.** I**ncidence of cancer in Brazil. 2020**. **Estimativa 2020. Estimativa de câncer no Brasil. [in Portuguese].** Available at: <https://www.inca.gov.br/publicacoes/livros/estimativa-2020-incidencia-de-cancer-no-brasil> Last accessed: 20 Sep. 2021.

[3] INCA – Instituto Nacioanal do Câncer (National Cancer Institute). **Breast câncer 2020**. **Câncer de mama. 2020 [in Portuguese].** Available in: https: //www.inca.gov.br/tipos-de-cancer/cancer-de-mama. Last accessed: 20 Sep. 2021.

[4] SANTOS, W. S.; NEVES, L. P.; PERINI, A. P.; SANTOS, C. J.; BELINATO, W.; SILVA, R. M. V.; SOARES, M. R.; VALERIANO, C. C.; CALDAS, L. V. E**.** Computational modeling of cervix uterus radiation procedure using a virtual anthropomorphic phantom and the MCNPX code. **J Phys Conf Ser.**, v.1, p.18-46, 2021.

[5] GONZALEZ, A. B. D.; CURTIS, R. E.; GILBERT, E.; BERG, C. D.; SMITH, S. A.; STOVALL, M.; RON, E**.** Second solid cancers after radiotherapy for breast cancer in seer cancer registries. **Br J Cancer.**, v. 102, p. 220–226, 2010.

[6] STOVALL, M.; SMITH, S. A.; LANGHOLZ, B. M.; JR, J. D. C.; SHORE, R. E.; ANDERSSON, M.; BUCHHOLZ, T. A.; CAPANU, M.; BERNSTEIN, L.; LYNCH, C. F.; MALONE, K. E.; ANTON-CULVER, H.; HAILE, R. W.; ROSENSTEIN, B. S .; REINER, A. S.; THOMAS, D. C.; BERNSTEIN, J. L. Dose to the contralateral breast from radiotherapy and risk of second primary breast cancer in the we care study. **Int J Radiat Oncol Biol Phys.**, v. 72, p. 1021–1030, 2008.

[7] HUANG, J.; MACKILLOP, W. J. Increased risk of soft tissue sarcoma after radiotherapy in women with breast carcinoma. **Cancer.**, v. 92, p. 172–180, 2001.

[8] KIROVA, Y. M.; RYCKE, Y.; GAMBOTTI, L.; PIERGA, J. Y.; ASSELAIN, B.; FOURQUET, A. Second malignancies after breast cancer: the impact of different treatment modalities. **Br J Cancer.**, v. 98, p. 870 – 874, 2008.

[9] PELOWITZ, D. B. **MCNPX User's Manual, version 2.7.0.** Report LA-CP-11-00438. Los Alamos National Laboratory, 2011.

[10] SILVEIRA, M.; CAMPOS, T. Radiodosimetric evaluation using the mcnp-5 code for radiosteoplasty in bone tumors in the limbs. **Rev Mat.,** v. 12, p. 186–92, 2007.

[11] MENDES, B. M.; TRINDADE, B. M.; FONSECA, T. C. F.; CAMPOS, T. P. R. Assessment of radiation-induced secondary cancer risk in the brazilian population from left-sided breast-3d-crt using mcnpx. **Br J Radiol**., v. 90, p. 20170187, 2017.

[12] TAGHAVI, R.; MIRZAEI, H. R.; AGHAMIRI, S. M. R.; HAJIAN, P. Calculating the absorbed dose by thyroid in breast cancer radiotherapy using mcnp-4c code. **Radiat Phys Chem.**, v. 130, p. 12–14, 2017.

[13] TOSSI, M. T.; MAHAMADIAN, N.; MOHAMMADI, M.; GHORBANI, M.; HASSANI, M.; KHAJETASH, B.; KHORSHIDI, F.; KNAUP, C. Assessment of skin dose in breast cancer radiotherapy: on-phantom measurement and Monte Carlo simulation. **Rep Pract Oncol Radiother.**, v. 25, p. 456-461, 2020.

[14] BEDNARZ, B.; XU, X. G. Monte Carlo modeling of a 6 and 18 MV Varian Clinac medical accelerator for in-field and out-of-field dose calculations: Development and validation. **Phys Med Biol.**, v. 54, p. 43-57, 2021.

[15] CASSOLA, V. F.; MILIAN, F. M.; KRAMER, R.; LIRA, C. A. B. de O.; KHOURY, H. J. Standing adult human phantoms based on 10th, 50th and 90th mass and height percentiles of male and female caucasian populations. **Phys Med Biol.**, v. 56, p. 3749, 2011.

[16] ICRP – International Commission on Radiological Protection. The 2007 Recommendations of the International Commission on Radiological Protection**.** 103 Publication. **Ann of the ICRP**, v.37, p. 2-4, 2007.

[17] SHEIKH-BAGHERI, D.; ROGERS, D. Monte Carlo calculation of nine megavoltage photon beam spectra using the beam code**. Med Phys.**, v. 29, p. 391–402, 2002.

[18] CATUSSO, L.; SANTOS, W. S.; DA SILVA R. M. V.; VALENÇA, J. V. B. Mobile shielding evaluation on the fetal dose during a breast radiotherapy using Monte Carlo simulation. **Phys Med**., v.84, p.24 – 32, 2021.

[19] RUDRA, S.; AL-HALLAQ, H. A.; FENG, C.; CHMURA, S. J.; HASAN, Y. Effect of RTOG breast / chest wall guidelines on dose-volume histogram parameters. **J Appl Clin Med Phys.**, v. 15, p. 127–137, 2014.

[20] FONSECA, E.; OLIVEIRA, C.; REBELLO, W.; MEDEIROS M. P.; FONSECA, C.; BAPTISTA, C. Calculation, using the code MCNPX, of equivalent doses in the 3D-CRT treatment

of prostate cancer, with gantry operating at 45 °, 135 °, 225 ° and 315 °. **Braz J Radiat Sci.**, v. 8, p. 11, 2020.

[21] SCHETTINO, R C.; JOTTA, L. M. G. N.; CASALI, G. D. Lung function in women with breast cancer undergoing radiation therapy: a pilot study. **Fisioter Pesq.**, v. 17, p. 248–252, 2010.

[22] HORMATI, A.; HAJIANI, E.; ALAVINEJAD, P.; SHAYESTEH, A. A.; MASJEDIZADEH, A. R.; HASHEMI, S. J. Evaluation of breast cancer radiotherapy induced liver fibrosis by elastography. **J Gastroenterol Hepatol Res**., v. 3, p.1026–1209, 2014.

[23] CARVALHO, H.; SALES C. P .; STUART S. R.; GIL, E.; NUNES, A. C. N.; FERAUCHE, D. C. Comparison between lung volumes irradiated with two-dimensional and three-dimensional techniques conformed to radiotherapy for patients with locally advanced lung tumors. **Radiol Bras**., v. 42, p. 303–308, 2009.

[24] BRENNER, D.; HUDA, W. Effective dose: A useful concept in diagnostic radiology? **Radiat Prot Dosimetry.**. v. 128, p. 503–508, 2008.

[25] National Research Council. **Health Risks from Exposure to Low Levels of Ionizing Radiation: BEIR VII Phase 2**. Washington, DC: The National Academies Press, 2006.